Korea-Australia Rheology Journal
Vol. 15, No. 4, December 2003 pp. 197-208

Global measures of distributive mixing and their behavior in chaotic flows

Charles L. Tucker III* and Gerrit W. M. Peters[1]
Department of Mechanical and Industrial Engineering, University of Illinois, Urbana, IL 61801 USA
[1]Materials Technology, Department of Mechanical Engineering, Eindhoven University of Technology 5600 MB Eindhoven, The Netherlands

(Received December 11, 2003)

Abstract

Two measures of distributive mixing are examined: the standard deviation σ and the maximum error E, among average concentrations of finite-sized samples. Curves of E versus sample size L are easily interpreted in terms of the size and intensity of the worst flaw in the mixture. $E(L)$ is sensitive to the size of this flaw, regardless of the overall size of the mixture. The measures are used to study distributive mixing for time-periodic flows in a rectangular cavity, using the mapping method. Globally chaotic flows display a well-defined asymptotic behavior: E and σ decrease exponentially with time, and the curves of $E(L)$ and $\sigma(L)$ achieve a self-similar shape. This behavior is independent of the initial configuration of the fluids. Flows with large islands do not show self-similarity, and the final mixing result is strongly dependent on the initial fluid configuration.

Keywords **:** mixing, chaotic mixing, mixing measures, cavity flow, mapping method

1. Introduction

In recent years, considerable attention has been focused on chaotic flows and their mixing behavior (Ottino, 1989; Aref and El Naschie, 1995). This field of study began from the realization that deterministic laminar flows can create chaotic motions (Aref, 1984), and we now understand that globally chaotic flows provide the most effective way to mix two fluids in a laminar flow. A variety of tools have been developed to examine and characterize chaotic flows, including Poincaré sections, periodic point analysis (Meleshko and Peters, 1996), and stretching distributions (Muzzio *et al.*, 1991; Liu *et al.*, 1994b). These tools provide rich insights into the nature of chaotic flows, and they reveal much about the mechanisms that make chaotic mixing so effective. However, none of these tools provides a direct description of the distributive mixing behavior of a given flow.

Before one can study distributive mixing, one must be able to measure it. Danckwerts (1952) introduced the scale and intensity of segregation, concepts that still provide the basis for examining and characterizing mixtures. However, Danckwerts considered only mixtures with no long-range segregation, and in distributive mixing it is precisely the long-range segregation we seek to eliminate. Thus, we need a meaningful way to quantify distributive mixing in the presence of long-range segregation. Only when one can answer questions like "Is A better mixed than B?" or "Is B sufficiently well mixed for my purposes?" will it be possible to assess and compare the mixing performance of different flows, chaotic or regular.

The goals of this paper are to define some useful global measures of distributive mixing, to show how they are related to the properties of mixtures, and to use them to explore the distributive mixing performance of some chaotic flows. Here, "distributive mixing" means any operation intended to create a uniform spatial arrangement of the constituents of a mixture, and "global" indicates that the measures characterize the *entire* mixture. Our exploration of chaotic flows will be limited to passive laminar mixing, i.e., the mixing of two fluids with identical rheology and zero interfacial tension. However, the measures of distributive mixing are independent of the physical phenomena used to create the mixture, and apply equally well to liquid-liquid mixtures containing droplets, to the dispersion of solid particles in a liquid, or to the mixing of granular solids.

The measures proposed here rely on knowing the entire mixture pattern. For example, if we are examining a batch mixing device, we must be able to determine the composition of the mixture at every point in the mixing cavity. While such information is available in principle from experiments - one could imagine solidifying the fluids *in situ* after mixing, and then measuring a large number of cross-sections - such experiments are seldom practical.

*Corresponding author: ctucker@uiuc.edu

However, some computational techniques do predict the composition of the entire mixture are each time during the mixing process (Chella and Viñals, 1996; Kruijt *et al.*, 2001; Galaktionov *et al.*, 2002a). We need a way to assess the results of such computations, and this is where the measures proposed here will be most useful.

The paper is organized as follows. Section 2 discusses the issue of length scales and introduces the two proposed measures of distributive mixing. This is followed in section 3 by a brief summary of the mapping method (Kruijt *et al.*, 2001), which is the technique used to create the various mixture patterns that are examined here. Section 4 examines a diverse set of mixture patterns, to see how the two measures capture and represent different features of distributive mixing. Following this, section 5 examines the time dependence of the measures in selected mixing flows, including asypmtotic behavior at long times and dependence on initial conditions. The paper closes with a short discussion and summary.

2. Measures of distributive mixing

2.1. Length scales of examination

Consider the mixture patterns shown in Fig. 1. We wish to choose some quantity that can be determined for each pattern, to describe its quality of mixing. This quantity should not depend on the history of the mixture or the mechanisms by which is was created, but only on the information present in the image. Accordingly, we defer explanation of the creation of these patterns until section 3, and focus on the information they contain.

The classical work of Danckwerts (1952) starts from the notion of *concentration at a point*, a viewpoint that makes a clear distinction between two length scales. The concentration at a point $c(x)$ is taken to be the average concentration over a region that is larger than the atomic scale, but smaller than the smallest droplet, striation, or particle in the mixture. In this view, which is consistent with classical continuum mechanics, the function $c(x)$ fully describes a particular mixture.

Danckwert's two measures, scale and intensity of segregation, are based on the autocorrelation function of $c(x)$. The use of two measures is based on a separation of length scales: scale of segregation is only altered by advection and deformation of the material (motions above the length scale of a point), while intensity of segregation is only altered by molecular diffusion (motions below the length scale of a point). However, Danckwerts' analysis was focused on the short-range properties of $c(x)$, and was limited to mixtures with no long-range segregation. In the present study we wish to describe this long-range segregation, separately from the local texture or microstructure of the mixture.

This separation is achieved by introducing a second length scale which, for lack of a better term, will be called the *cell size*. The cell size is much larger than the desired final microstructure of the mixture, but much smaller than the mixture's overall size. In a numerical simulation, the cell size might be the size of the grid or mesh used to represent the entire mixture, or it might be a length scale over which the velocity gradient is approximately constant.

Using the cell size, we can characterize the mixture on two levels:

the macrostructure where the smallest object examined is a cell, and the largest is the entire mixture.
the microstructure where the smallest object examined is a continuum point, and the largest is a cell.

Most traditional measures of mixing are ways of describing microstructure, also called the morphology or texture. Danckwerts' scale and intesity of segregation belong to this group, as do striation thickness (Mohr *et al.*, 1957), area tensors (Wetzel and Tucker, 1999), and droplet size distributions. In the present view we regard the microstructure as a local property that characterizes a region on the order of the cell size. A specific microstructure is described by the concentration function $c(x)$, and all microstructural descriptors can be extracted from this function.

In contrast, a specific macrostructure is described by cell-average values, or coarse-grain concentrations. For distributive mixing the relevant quantity is the volume-average concentration of a cell, $C(x)$:

$$C(x) = \frac{1}{V_{cell}} \int_{V_{cell}(x)} c \, dV \tag{1}$$

Each mixture pattern in Fig. 1 consists of an array of 120 by 200 square cells. The gray level of each cell is proportional to C, with $C = 0$ corresponding to black and $C = 1$ corresponding to white. While the pointwise concentration c can differ from one or zero only through the action of molecular diffusion, fluid motion can make $0 < C < 1$, whenever a cell contains both black and white fluid. Values of C are exactly the type of information that is available from direct numerical simulations of mixing. In principle one could compute $C(x)$ as a continuous function of x, but in practice one may have values only for discrete cells. From these values we wish to extract measures that describe the important features of the macrostructure.

The complete characterization of any mixture must include measures of both macroscopic and microscopic mixing. In another publication we have described a model that predicts mixing behavior at both scales (Galaktionov *et al.*, 2002b). The remainder of this discussion will focus on macroscopic, or distributive, mixing.

2.2. Proposed measures

The purpose of distributive mixing is to create a uniform

macrostructure. One might simply say that we want to make $C \approx \bar{c}$ for all cells, where $\bar{c}$ is the average concentration for the entire mixture. However, this would tie the mixing measure to the cell size, which might well differ from simulation to simulation, and will certainly change its physical size if we scale up the mixer.

To handle this scaling issue we introduce an averaging volume V_{avg}, whose size is characterized by a length L. The first step in assessing a mixture is to calculate the average concentration for each averaging volume. We denote the average concentration for the i^{th} averaging volume V_i by $\langle C\rangle_i$ Thus,

$$\langle C\rangle_i = \frac{1}{V_{avg}} \int_{V_i} C \, dV \tag{2}$$

Since the $\langle C\rangle_i$'s are computed from the C's, we must have $V_{avg} \geq V_{cell}$. Indeed, one cannot determine information on any scale smaller than the cell size when the only data available are the cell values of C.

Once the averaging volume has been chosen and the $\langle C\rangle_i$ values computed, the mixture is characterized by the statistical properties of $\langle C\rangle$. A perfectly distributed mixture is defined as one in which $\langle C\rangle_i = \bar{c}$ for all i. Appropriate measures of distributive mixing should then describe how far the $\langle C\rangle_i$'s deviate from $\bar{c}$. A traditional measure is the sample standard deviation,

$$\sigma(L) = \sqrt{\frac{1}{M}\sum_{i=1}^{M}(\langle C\rangle_i - \bar{c})^2} \tag{3}$$

We write σ as a function of L, since its value for any mixture will depend on the size (and shape) of the averaging volume.

While σ is a robust statistic that draws information from every averaging volume, it is not sensitive to the situation in which only a few averaging volumes differ significantly from the desired value. Yet this situation is quite important, since the quality of a mixture is often determined by a few poorly-mixed spots. Therefore, as a second measure of distributive mixing we propose the maximum sample error E, which is the maximum deviation of any averaging volume from the global mean:

$$E(L) \equiv \max\left|\langle C\rangle_i - \bar{c}\right| \tag{4}$$

Again the notation emphasizes that E depends on L. We will see that $E(L)$, while not radically different from $\sigma(L)$, does make some features of the mixture pattern more readily apparent.

Both E and σ lend themselves well to answering the question "When is the distributive mixing good enough?" For any application one should be able to choose a critical sample size L^* and critical deviations E^* and σ^*, such that any mixture with $E(L^*) \leq E^*$ and/or $\sigma(L^*) \leq \sigma^*$ possesses adequate distributive mixing. These criteria guarantee that no sample of size L^* will have too large a deviation from the desired mean composition. Of course these are macroscopic criteria; in practice it may also be important to satisfy other criteria for adequate microscale mixing.

The size and shape of the averaging volume matter, but the measures are insensitive to the distribution of material *within* the averaging volume. A mixture that has a checkerboard pattern of individual cells is, by this definition, perfectly distributed if V_{avg} is a square of two cells by two cells, but perfectly segregated if V_{avg} is a single cell. One can only say that a given pattern is well mixed *after* an averaging volume has been chosen. For this reason, it makes sense to examine any mixtures using a range of sample sizes.

The sample variance σ^2 has long been used as a measure of mixing quality (Danckwerts, 1952; Scott and Bridgwater, 1974; Tucker, 1981), and it is often normalized by its value for a completely segregated mixture, $\bar{c}(1-\bar{c})$. We use $\sigma(L)$ in its dimensional form here to facilitate comparisons with $E(L)$.

Several analyses have shown that the sample variance can be derived from the correlation function for $c(x)$ (Scott and Bridgwater, 1974; Tucker, 1981). These analyses reassure us that, by computing $\sigma(L)$ or $E(L)$ for large samples, we are taking into account the correlations in composition between nearby cells. However, these analyses all begin with the assumption of uniform statistical properties across the entire measurement area. Thus, they cannot be applied to the present case, where we have no a *priori* expectation of statistical uniformity. Sample variance analysis, and the relationship between sample variance and scale of segregation (Danckwerts, 1952), are useful only in the analysis and measurement of mixtures on the microstructural level.

3. Generation of mixture patterns

We consider mixing in 2-D time-periodic flows in a rectangular cavity with upper and lower moving walls. Many aspects of mixing in this flow have been studied, both experimentally and theoretically (Chien *et al.*, 1986; Leong and Ottino, 1989; Ottino, 1989; Liu *et al.*, 1994b,a; Meleshko and Peters, 1996). The mixture patterns examined here were generated using the mapping method of Kruijt, Galaktionov, Anderson, Peters, and Meijer (2001). The mapping method treats passive mixing, i.e., the mixing of two fluids with equal viscosity and no interfacial tension, in laminar flow. All cases examined here concern the creeping flow of a Newtonian fluid, and use a rapidly-converging series solution for the velocity field (Meleshko, 1996). The cavity has a height to width ratio of 3/5.

Briefly, the mapping method works as follows. The cavity is divided into cells, in this case an array of 120×200 square cells. A few particular values for the displacement of the moving wall are chosen. Here we use dimensionless displacement values D of 1, 2, and 4. These lengths are

scaled by the half-width of the cavity, so $D = 2$ means that a point on the moving wall that begins at the upper left-hand corner of the cavity will translate to the upper right-hand corner. For each value of D the displacement and deformation of the cell boundaries is calculated, using an adaptive interface tracking method. This method tracks the position of multiple points on the cell boundary and adds points adaptively, allowing the displaced boundaries to be found for large deformations (Galaktionov *et al.*, 2000).

The displaced and distorted cells are overlaid on the original cell pattern, and the components of the mapping matrix $[\Phi]$ are calculated such that Φ_{ij} equals the area of the deformed cell j that lies on top of undeformed cell i. Finding Φ for each displacement is a demanding calculation that is done once, off line, and the results are stored for later use.

The mixing simulation then proceeds in a stepwise fashion. The initial pattern for each step is represented by a set of initial cell concentrations C_j on the undeformed cells. The C value in any cell is, of course, maintained as the cell is distorted, but at the end of the step the mapping calculation transfers this information back to the undeformed cells according to

$$C_i^{new} = \sum_j \Phi_{ij} C_j \tag{5}$$

Each succeeding step is found by repeating this multiplication, inserting the previous result for C_i^{new} on the right-hand side. The matrix $[\Phi]$ is large (in this case 24,000 × 24,000), but sparse. With an appropriate sparse matrix algorithm each multiplication of Eqn. (5) can be done quite rapidly.

The mixtures in Fig. 1 all begin from an initial condition of white fluid in the left half of the cavity, and black fluid on the right. This is the initial condition for all subsequent data, except when stated otherwise.

A mixing protocol consists of a periodic sequence of motions of the top and bottom walls, either to the left or to the right. Each step in the protocol uses one or more multiplications like Eqn. (5) to accumulate the necessary wall displacement. The different sequences of top and bottom motion studied here are listed in Table 1. Individual protocols are indicated by a letter from this table, indicating the sequence of steps, and by the dimensionless displacement taken at each step. Thus, one period of protocol B8 consists of moving the top wall 8 units to the right, and then moving the bottom wall 8 units to the left.

Table 1. Protocols used to generate example mixtures. T denotes motion of the top wall to the right, and B motion of the bottom wall to the left. $(-T)$ and $(-B)$ are top and bottom motions in the opposite directions

Protocol	Step Sequence
A	T
B	TB
C	TBTB BTBT
D	TBBT BTTB BTTB TBBT
E	TB(-T)(-B)

The total displacement D_{tot} is the sum of the absolute values of the displacements D for each step, and is proportional to the amount of work done in deforming the mixture. Since we only consider creeping flows here, the displacement of the fluid and the amount of mixing depend only on D_{tot}, and not on the velocity of the motion. Thus, D_{tot} is a convenient and appropriate measure of mixing time. All of the patterns in Fig. 1 have a dimensionless total displacement of 128, where again we non-dimensionalize by one half of the cavity width. The dramatic differences between the patterns in Fig. 1 show clearly that, although the total work is the same, different protocols have very different mixing behavior.

The mapping method only resolves the distribution of

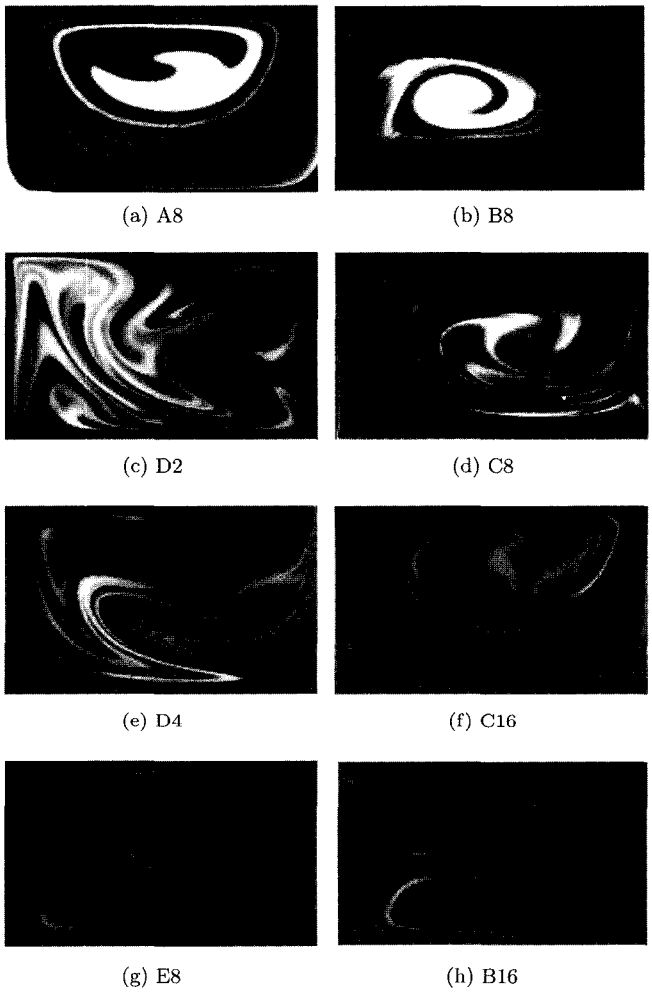

Fig. 1. Example mixtures, created using protocols from Table 1. All mixtures in this figure have a total dimensionless displacement of 128.

material on the scale of the cell size, so it will smooth out differences in concentration that are sharper than this. The effect can be seen, for example, in mixture A8 in Fig. 1(a). The large black and white regions in the center of this mixture should meet at a sharp border, but there is a thin gray region in between that smooths the transition.

This smoothing also introduces errors in the transport of the material. During each mapping step, material from a donor cell j is distributed into several recipient cells, according to the coefficients Φ_{ij} in the mapping matrix. In reality, a specific portion of cell j is transported to one recipient, and other portions are transported to other recipients. If the donor cell j contains a mixture of black and white fluid, the exact solution may be that some recipient cells should receive only black fluid, and some should receive only white. But in the mapping method all recipients are given the cell average concentration C_j. This effect gradually smooths out concentration differences between cells, and we will refer to it as numerical diffusion.

The numerical diffusion present in the mapping method is neither uniform in space nor isotropic, and analyzing its influence is a difficult task. For the present we simply note that the desired result of distributive mixing is to transform all cells from their initial black and white colors to a uniform gray, and in the mapping calculation this occurs by two mechanisms: transport of both black and white fluid into a cell, and numerical diffusion. The first mechanism is the physical process we wish to model, and the second mechanism is a numerical artifact that is inherent in the calculation. When we study time-dependent behavior of the mixture measures in section 5, we will want to be aware of this numerical artifact when interpreting the results.

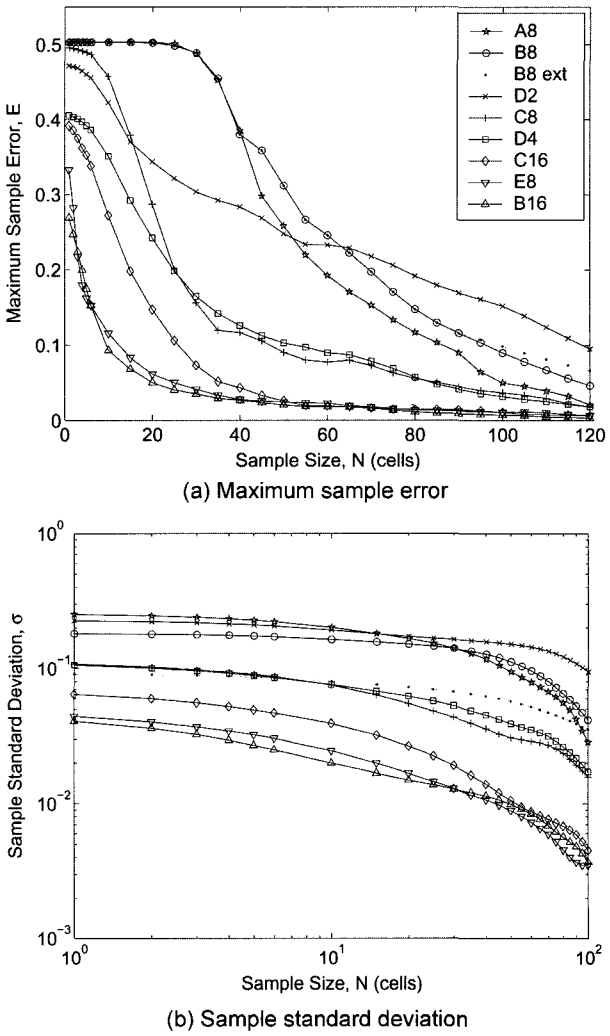

Fig. 2. Distributive mixing measures for the example mixtures in Figs. 1 and 3.

4. Measures for example mixtures

To demonstate the properties of $E(L)$ and $\sigma(L)$, we apply them to the two-dimensional mixtures shown in Fig. 1. The results of the mapping calculation provide the value of C for each cell.

For present purposes a compact averaging volume seems appropriate, so the averaging volume is chosen to be a square of $N \times N$ cells. L is taken as the length of an edge of this square, and its value (in the same dimensionless units used to describe wall displacement) is $N/100$. Values of E and σ are computed for a variety of sample sizes and reported as $E(N)$ and $\sigma(N)$, using values of N ranging from one to 120.

The sample concentrations $\langle C \rangle_i$ for each N were computed using a moving average. That is, the averaging window was placed over the top left corner of the image and a value of $\langle C \rangle_i$ was computed. Then the window was moved to the right by one cell and another value computed, and so forth. The $\langle C \rangle_i$ values are actually computed using fast Fourier transform methods. For any value of N this produces an array of $(200 - N + 1) \times (120 - N + 1)$ values of $\langle C \rangle$. $E(N)$ and $\sigma(N)$ are then extracted from these values.

Fig. 2 shows the measures for the mixtures from Fig. 1. Looking at results for $E(L)$ in Fig. 2(a), we find many interesting features. First, as one might expect, E tends to decrease with increasing N, and better distributive mixing corresponds to lower values of E. The ordering of the curves in Fig. 2(a) generally matches one's visual impressions of the mixtures in Fig. 1.

Second, the presence of a distinct bad spot, or island, in the mixture appears as a flat spot in the curve at small N. The curve starts to drop (exhibits a "knee") at a value of N on the order of the island size. Mixtures A8 and B8 both have islands that are about 30 cells wide, while mixture C8 has an island about 10 cells wide. Mixtures E8 and B16 have no islands, or at least none larger than the cell size; for these mixtures the curve of $E(N)$ exhibits a downward

slope between $N = 1$ and $N = 2$.

The maximum sample error E allows mixtures with very dissimilar macrostructure to be compared. Mixtures A8 and B8 are not at all similar in appearance, but in terms of $E(N)$ they have quite similar quality of distributive mixing. This ability to make quantitative and unambiguous comparisons is precisely what one seeks from a mixing measure. However, the scale of observation, L or N, must be specified before it is possible to say that one mixture is better than another. For any $N \geq 25$, we would say that mixtures C8 and D4 are quite similar, and that mixture C16 is better. But if we chose $N = 1$ then D4 is as good as C16, and both mixtures are much better than C8. Looking again at Fig. 1, we see that D4 and C16 have streaks of unmixed material that are similar in width, while C8 has a somewhat larger blob of poorly mixed material. The sample error E is sensitive to the sizes of these blobs or streaks.

Similarly, if we compare mixture D2 to mixtures A8 and B8, we see that D2 is noticeably better for $N < 40$, but noticeable worse for $N > 70$. This is due to a long-range segregation in mixture D2, which on the average is darker on the right and lighter on the left. These examples emphasize the importance of the averaging volume size in assessing distributive mixing.

The standard deviation curves in Fig. 2(b) are smoother than the curves for E, because standard deviation is a more robust statistic, but they offer less information to interpret the characteristics of the mixture. The $\sigma(N)$ results generally rank the mixtures in the same way as $E(N)$. However, if we looked only at $\sigma(N)$ for $N < 10$, we would say that mixtures C8 and D4 are equivalent, and that C16 is better. The standard deviation is not as sensitive as E to the small poorly-mixed streaks in C16, because it averages data from the entire mixture, and many of the cells in C16 are quite well mixed. In a similar way, the standard deviation gives a different relative assessment of mixtures A8, B8, and D2, saying that B8 is better mixed than D2 for small N. Both measures agree that D2 is the least well distributed on large scales, but the crossover comes at $N = 20$ for σ and at much higher values for E.

An important difference between the two measures is that E is sensitive to the absolute size and composition of the worst spot, regardless of the overall size of the mixture. In contrast, σ loses track of a fixed-size flaw as the overall size of the mixture is increased. To illustrate this point, we extend pattern B8 by embedding it in the center of an array of 240 by 400 cells, setting the concentrations of all the new cells to the average of the original B8 pattern. This extended pattern, shown in Fig. 3, has four times the area of the original B8 pattern, assuming that the cell size is constant. The curve for $E(N)$ for this mixture, shown in Fig. 2(a), is unchanged except for very large sample sizes. We can still see, in the early shape of the curve, the presence and size of the island. In contrast, the $\sigma(N)$ curve for the new mixture (Fig. 2(b)) is considerably lower than the original B8 curve, giving the impression that the extended

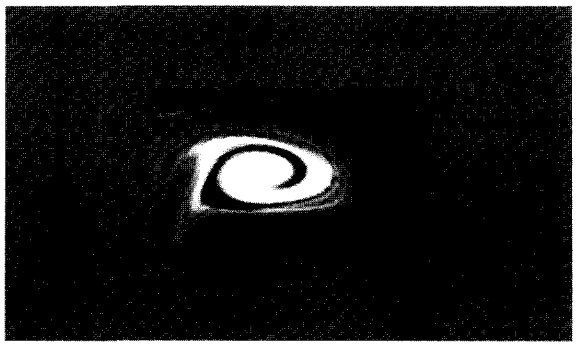

Fig. 3. B8 mixture pattern, extended to a total size of 240 by 400 cells. Data for this pattern is labeled "B8 ext" in Fig. 2.

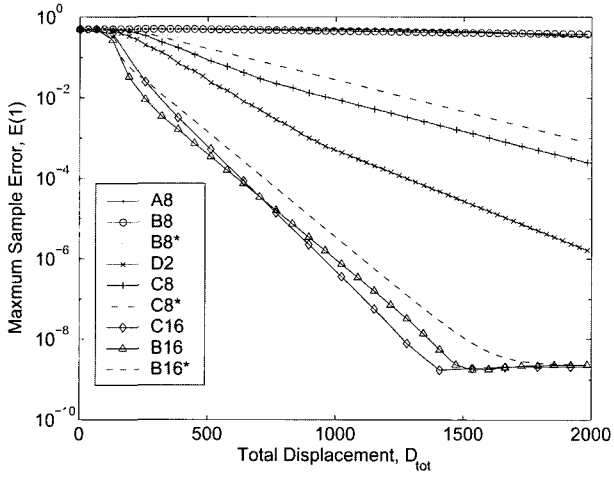

(a) Maximum sample error

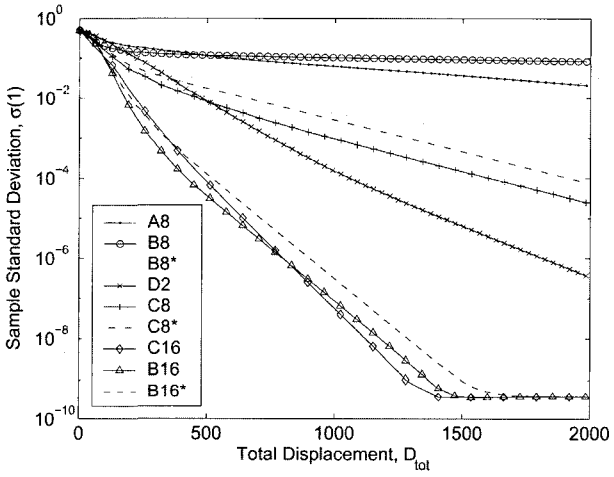

(b) Standard deviation

Fig. 4. Mixture measures for $N = 1$ versus total displacement for different protocols. The curves labeled B8*, C8*, and B16* start with white fluid in the top half of the cavity and black fluid in the bottom half; all other data uses a left/right initial condition.

B8 pattern is somehow better mixed than before. This is hardly the case, since from either pattern we can draw out a sample whose composition is far from $\bar{c}$.

5. Time dependent behavior

The mixing measures E and σ can be used to study how distributive mixing develops with time in the time-periodic cavity flows described in Table 1. Fig. 4 shows E and σ for $N = 1$, plotted against total displacement of the upper and lower walls D_{tot}, for selected protocols from Fig. 1. The curves for mixtures D4 and E8, which are not shown, are very similar to the curves for C16 and B16. Note that the images in Fig. 1 correspond to a total displacement of D_{tot} = 128, while the curves of Fig. 4 begin at zero displacement and continue to very large values. Recall that D_{tot} is the proper measure of time, or mixing effort, for these creeping flows.

As one might expect, the general trend is for all curves in Fig. 4 to decrease with time. However, the various mixing protocols behave quite differently from one another. Protocols C16 and B16 mix rapidly and exhibit steep curves, protocols A8 and B8 mix very slowly and have at curves, while protocols D2 and C8 fall in between.

The curves for protocols C16 and B16 bottom out in the vicinity of E or σ equal to 10^{-9}. This is a numerical artifact of the mapping method, not a physical behavior. At this point in the calculation all cells have almost the same value C, and the distributive mixing is almost perfect. However, because of roundoff errors in the mapping computation, Eqn. (5), there is always a small amount of variation among the C's, which we can see in Fig. 4 because of the logarithmic axis. If the precision of the mapping calculation were increased the curves would continue downwards, but would eventually flatten again at some lower level. Of course, a value of E or σ less than, say, 10^{-2} might be adequate mixing for many purposes, while a value less that 10^{-4} would be hard to detect experimentally, and should represent sufficient distributive mixing for almost any purpose. The curves flatten well below these values, so the present calculations have adequate numerical precision. The bottoming of the curve simply signals the end of the meaningful data from the mapping calculation.

5.1. Chaotic flows

An important feature of Fig. 4 is that the data for several protocols achieve constant slopes on this semi-logarthmic plot, implying that these protocols possess a long-time asymptotic behavior in which E and σ decrease exponentially with time. A careful examination of the data shows that E decreases with the same exponent as σ for protocols D2, C8, C16, and B16. E and σ are different statistics for the distribution of sample values $\langle C \rangle$, so the fact that both statistics decrease at the same rate implies that the distribution of cell values is changing in a self-similar way.

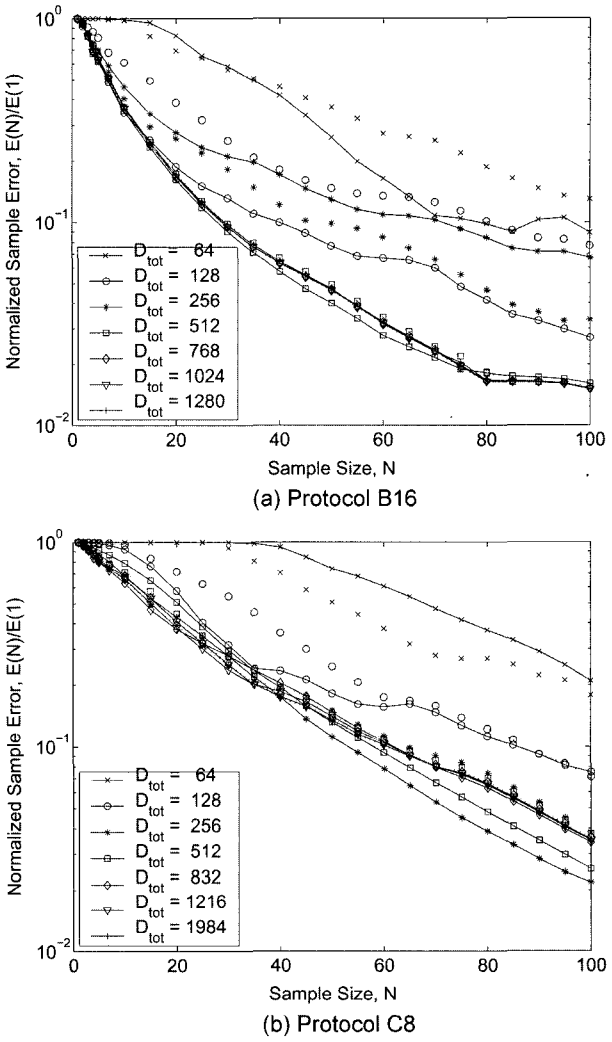

Fig. 5. Normalized sample error $E(N)/E(1)$ for chaotic protocols. As total displacement D_{tot} increases, the curves for each protocol converge to a single shape. Dotted lines connect data for the top/bottom initial condition; solid lines are for the left/right initial condition.

This self-similarity is demonstrated in Fig. 5 for protocols B16 and C8. Here the data for $E(N)$ at each value of displacement are divided by the current value of $E(1)$ so that, once the curves achieve a self-similar shape, the data for different total displacements should superimpose. Indeed this is what we observe in Fig. 5. For protocol B16 the curve is very close to the asymptotic result when D_{tot} equals 512, and for D_{tot} = 768 to 1280 the superposition is almost perfect. Protocol C8 mixes more slowly, so the asypmtotic behavior is reached at somewhat higher values of total displacement. The curves for $\sigma(N)/\sigma(1)$ exhibit the same behavior, so this data is not shown. Note that the normalizing factor $E(1)$ decreases with time, causing some of the curves in Fig. 5 to lie below the asymptotic curve. However, the actual values of $E(N)$ decrease monotonically

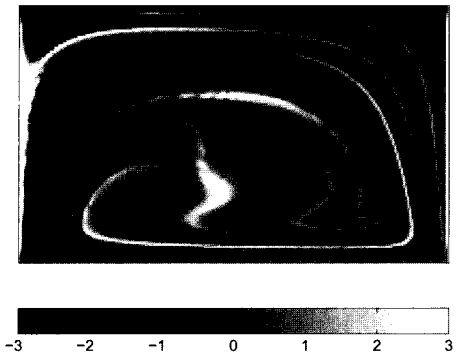

(a) $D_{\text{tot}} = 512$, $\sigma = 3.10 \times 10^{-5}$

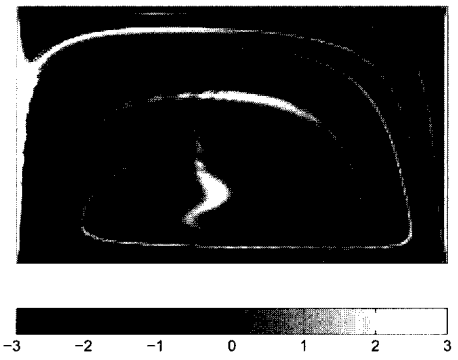

(b) $D_{\text{tot}} = 1024$, $\sigma = 6.53 \times 10^{-8}$

Fig. 6. Self-similarity of the scaled concentration deviation $(C - \overline{C})/\sigma$ for protocol B16. The initial condition is white on the left and black on the right.

with D_{tot}, like the curves in Fig. 4.

Fig. 6 provides a visual display of this self-similarity. Here we show the B16 mixtures for D_{tot} equal to 512 and 1024, both of which are in the region of asymptotic behavior. If these images were plotted using the values of C on a scale from 0 to 1, both pictures would be uniformly gray. To expose the small variations in concentration, Fig. 6 plots $(C - \overline{C})/\sigma$, the deviation in cell concentration from the mean, normalized by the standard deviation among all cells. While the standard deviation differs greatly between the two figures, the spatial patterns of the normalized concentration deviation are identical.

An important implication of self-similarity in $E(N)$ is that the exponential decrease with time is independent of the sample size, N or L. If we added curves for other values of N to Fig. 4, they would fall below the curves for $E(1)$, but would asymptote to straight lines with the same slope. The exponential decrease of E and σ is an intrinsic behavior of a particular globally chaotic flow, and does not depend on the sample size used to assess the quality of mixing.

We can now summarize the asymptotic behavior of E and σ as follows:

$$E(L, D_{tot}) = k_E \hat{E}(L) e^{-D_{tot}/\lambda} \qquad \sigma(L, D_{tot}) = k_\sigma \hat{\sigma}(L) e^{-D_{tot}/\lambda} \tag{6}$$

λ is a characteristic time constant, expressed here in units of dimensionless total displacement. The functions $\hat{E}(L)$ and $\hat{\sigma}(L)$ represent the asymptotic mixing measure curves as observed in Fig. 5, and k_E and k_σ are constants. We will see in a moment that the details of this asymptotic behavior are affected by numerical diffusion in the mapping calculation.

The exponential decrease in the mixture measures, and the self-similarity in the mixture patterns and mixture measures, are expected consequences of a globally chaotic flow. The mapping results for protocols B16, C16, C8, and D2 all exhibit these behaviors. A true globally chaotic flow would have no islands, and hence no regular regions. The protocols studied here may contain some small islands. However, if the islands are of the same order or smaller than the cell size, then they will be invisible to the mapping method, and the mapping calculation will behave as if the flow were globally chaotic. We will henceforth use "globally chaotic" in this looser sense. Fig. 4 shows clearly that not all chaotic protocols are equally effective at mixing. Protocols B16 and C16 give very similar mixing performance, while protocols D2 and C8 mix at a significantly lower rate.

5.2. Dependence on initial conditions

For globally chaotic protocols, the rate of exponential decrease of E and σ, and the asymptotic shape of the $E(L)$ curve, are independent of the initial condition. To show this, the calculations for protocols B16 and C8 were repeated with an initial condition of white fluid in the top half of the cavity and black fluid in the bottom half. The curves labeled C8* and B16* in Fig. 4, and the data connected by dotted lines in Fig. 5, are for this initial condition. In Fig. 4 we see that during the early stages of mixing the B16* curve is somewhat different than the B16 data, but when the curves reach their asymptotic behavior they have the same slope, indicating that they have the same time constant λ. The C8* and C8 curves also asymptote to the same slope.

Similarly, the normalized $E(N)$ data in Fig. 5(a) is quite different from the top/bottom initial condition in the early stages of mixing. However, by the time D_{tot} equals 512 the top/bottom data is very close to the asymptotic curve, and data from higher total displacements falls directly on top of the data for the first initial condition. Fig. 5(b) shows the same behavior for protocol C8, though the shape of the asymptotic curve is different.

In terms of Eqn. (6), the only factors affected by the initial configuration of the fluids are k_E and k_σ. The time constant λ and the functions $\hat{E}(L)$ and $\hat{\sigma}(L)$ are intrinisic properties of the mixing protocol.

Fig. 7 shows the concentration deviations for this initial

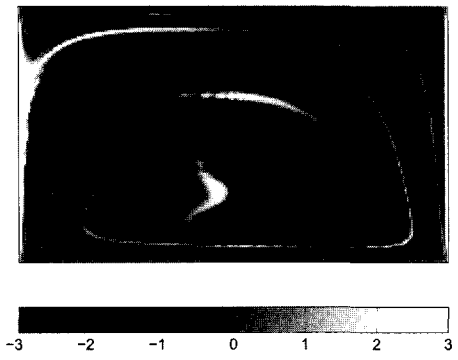

(a) $D_{\mathrm{tot}} = 512$, $\sigma = 1.07 \times 10^{-4}$

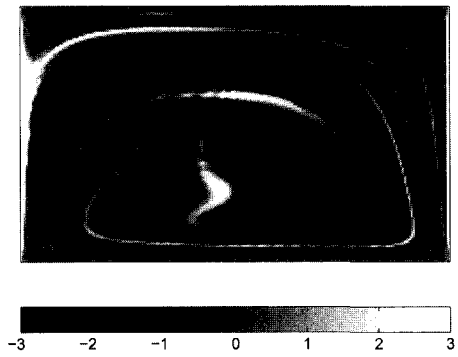

(b) $D_{\mathrm{tot}} = 1024$, $\sigma = 2.33 \times 10^{-7}$

Fig. 7. Self-similar scaled concentration deviations $(C - \overline{C})/\sigma$ for protocol B16*. Same as Fig. 6, but the initial condition is black on the top and white on the bottom.

condition, on the same normalized scale as in Fig. 6. Again the figures for the two values of D_{tot} are identical. The two images in Fig. 7 are also nearly identical to Fig. 6.

5.3. Regular protocols

In a periodic flow, a regular region (i.e., an island) is one in which each fluid particle returns, at the end of each period, to some location on a fixed orbit. Protocol A8, in which the top wall moves only to the right, is completely regular, since the flow is steady and each particle circulates on a fixed streamline. Protocol B8 has a large regular island, readily visible in Fig. 1, which surrounds a first-order elliptic point. There are also three smaller third-order islands surrounding the larger one (Kruijt *et al.*, 2001). We will call flows like A8 or B8 regular protocols, even though the region outside the islands in B8 is chaotic.

Physically, the fluid in an island does not communicate with the rest of the mixture, but remains within the island boundaries for all time. There may well be stirring inside the island, though the interfacial area within the island will grow linearly rather than exponentially. This may eventually lead to an even distribution of the two fluids within the island. However, the overall composition of the island is fixed by the initial configuration of the fluids, and does not change with time. If the island is initially off-ratio on average, the best that can be done is to give this island-average concentration to every cell in the island. As the island becomes homogeneous, and the chaotic regions also become well mixed, the measures $E(L)$ and $\sigma(L)$ should asymptote to constant values, which will depend on the initial configuration of the fluids.

The numerical behavior of the mapping method will be somewhat different from this physical behavior, especially at long times. The numerical diffusion present in the mapping method causes the calculation to slowly exchange material between the island and the remaining, chaotic regions of the flow. This occurs because some cells straddle the island boundaries, and the homogenization of the cell after each mapping step transfers material between the regular and the chaotic regions. As a consequence, $E(L)$ and $\sigma(L)$ as computed by mapping do not level off at constant values, but continue to decrease slowly.

This effect is evident in Fig. 4, where the curves for the regular protocols A8 and B8 decrease 12 very slowly compared to the chaotic protocols. The curve labeled B8* is for the top/bottom initial condition. This curve drops much more rapidly, until it finally levels out around $D_{tot} = 1500$. The top/bottom initial condition results in a much better final mixture for protocol B8 than the left/right initial condition, because the top/bottom initial condition places nearly equal amounts of black and white fluid in this particular island.

The presence of the island also eliminates the self-similarity of the $E(N)$ and $\sigma(N)$ curves. Fig. 8 shows the normalized data $E(N)$=$E(1)$ for protocol B8 at various times.

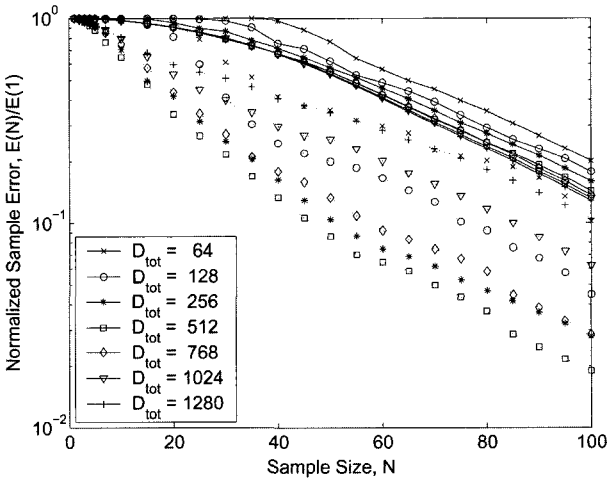

Fig. 8. Normalized sample error, $E(N)/E(1)$, for the regular protocol B8 at different values of total displacement D_{tot}, showing that self-similarity does not occur in this regular protocol. Dotted lines connect data for the top/bottom initial condition.

The data for the left/right initial condition (connected by the solid lines) appears to be approaching a constant shape, but the date for the top/bottom initial condition (the dotted lines) does not achieve the same shape.

This loss of self-similarity implies that for regular protocols the asymptotic slopes for E and σ are not the same. That is, while E and σ may both exhibit a slow exponential decline due to numerical diffusion, they do not decay at the same rate. This result is observed for both the A8 and B8 protocols in the data of Fig. 4, and is another signature of the presence of a large regular region in the flow.

5.4. Numerical diffusion in chaotic protocols

While we cannot eliminate numerical diffusion from the mapping calculation, we can explore its inuence on the results by increasing the amount of diffusion. This is accomplished by using a smaller step size D to accumulate the same total displacement, where D is the dimensionless displacement of the moving wall for an individual mapping step. All of the results so far, except for protocol $D2$, use only the mapping matrix for $D = 4$. If the same results are computed using a mapping matrix for $D = 2$, then there are twice as many steps in the calculation and the diffusion is increased.

Fig. 9 shows the behavior of $E(1)$ versus D_{tot} for protocols B16, C8, and B8, using D values of 4, 2, and 1. For protocol B16 the early parts of the curves for different D's are very similar. However, as mixing improves the results for smaller D fall away faster, and their asymptotic slope is significantly steeper. All of the calculations for B16 bottom out at about the same level, but this level is reached sooner when the numerical diffusion is larger. Similar behavior is observed for the other globally chaotic protocol, C8. Here the slope is quite a bit shallower, and the differences caused by numerical diffusion are smaller. While numerical diffusion has a distinct inuence on the results of the calculation, it still does not obscure the difference between protocols B16 and C8. The results for the regular protocol B8 also show a slope change due to numerical diffusion, though of course the mixing is never very good in this case.

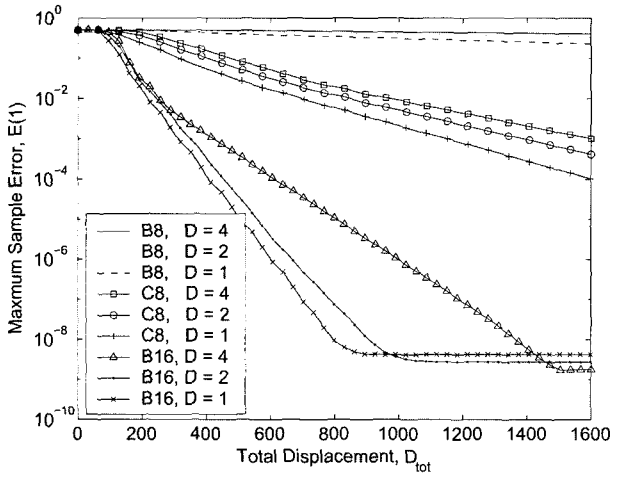

Fig. 9. Effect of numerical diffusion on $E(1)$. Numerical diffusion increases as D, the displacement of the individual mapping step, decreases.

From these results we conclude that the asymptotic slope of E in mapping calculations is inuenced by numerical diffusion, and that we should not attach too much significance to the numerical value of λ produced by the calculations. This raises an important qualification on all of the observations in this section: they apply rigorously only to the mapping calculation, and we have not proved that the physical mixing flow will have all of the same behaviors.

From the point of view of demonstrating the use of E and σ as mixing measures this presents no problem. The mapping calculation itself represents an interesting dynamical system, albeit an artificial one, that produces spatial mixture patterns. Clearly E and σ are useful tools for analyzing and describing the distributive mixing properties of the mapping method.

From the scientific point of view these results raise the interesting possibility that chaotic time-periodic fluid flows may exhibit the same asymptotic behavior, presumably with a somewhat larger value of λ than is predicted by the mapping method. Determining whether this conjecture is true requires some other type of calculation. However, a better calculation is difficult to do. As a simple example, one might imagine placing a large number of tracer particles in the flow, marking each one black or white according to its initial location, and following the particle motion over time. At any time one could average the concentration of all particles in a cell to get the cell value for C, and then analyze the distributive mixing state by finding $E(L)$ and $\sigma(L)$.

Similar "box counting" calculations have been performed by Jones (1991) and Liu *et al.* (1994a), however those calculations provide only a coarse measure of material distribution. Resolving the asymptotic behavior of σ and E would require tracking an extremely large number of points. If each cell contained n tracer particles whose colors were selected at random, then the standard deviation among the cell values would be $\sqrt{\bar{c}(1-\bar{c})/n}$; this is the resolution for σ with this method. From Fig. 9 we see that the asymptotic region begins at around $\sigma = 10^{-3}$. Achieving this resolution with the current grid of 24,000 cells would require tracking the paths of more than 10^{10} particles. To date, tracking 10^6 particles is about the largest calculation that is typically done today. If we actually wanted to obtain an accurate value for λ, this might require resolving the variance to within 10^{-4}, which pushes the number of particles over 10^{12}.

In contrast, each of the mapping calculations reported here is done in less than a minute on a personal computer. The mapping method provides a convenient and powerful

tool that can rapidly compare different protocols, and that can carry the mixing calculation forward to very high levels of homogeneity. It is these characteristics that have made the present exploration of distributive mixing possible.

6. Summary

This paper had two goals: to define meaningful measures of distributive mixing, and to demonstrate their application in the study of chaotic mixing.

In defining mixing measures, we began by choosing a length scale, the cell size, to separate the macroscopic and microscopic aspects of the mixture structure. The underlying data for the macrostructure consists of cell-average concentrations. The goal of distributive mixing is to make the average concentration in some finite-size sample approximately equal to the global average concentration, for any sample location in the mixture. This sample size may be the cell size, or it may be much larger.

Two measures of distributive mixing were proposed and examined: the standard deviation among samples σ, and the maximum sample error E. Both measures are closely related to the goal of distributive mixing, in that a small value of either means that the cell concentrations are nearly uniform.

The maximum sample error is more sensitive to the presence of a few poorly-mixed spots, and the curve of E versus sample size is readily interpreted in terms of the size and concentration in the bad spot. Maximum sample error is also insensitive to the size of the bad spot relative to the overall size of the mixture; a small uniform mixture with one bad spot, and a larger uniform mixture with the same bad spot, will have nearly identical values of maximum sample error. The disadvantage of E is that it requires knowing the concentration everywhere in the mixture. In this regard it is most useful for assessing numerical simulation results, while σ may be more useful for experiments.

Both E and σ provide the ability to compare mixture patterns that may be quite different in appearance, and to say which mixture is better distributed. Both measures can be applied to determine whether or not a pattern is suficiently well mixed for a given purpose. Either determination depends on the sample size, which must be chosen to suit the application. Both measures can be applied at any stage of the mixing process, from completely segregated to completely homogenized mixtures.

The two mixing measures were used to examine the distributive mixing behavior for time-periodic flows in a rectangular cavity. The mixing patterns were calculated using the mapping method, which has finite spatial resolution and a certain amount of numerical diffusion. The mapping method is limited to fluids with homogeneous rheological properties and no interfacial tension; here we consider creeping flows of Newtonian fluids. A variety of protocols, involving time-periodic sliding motions of the upper and lower cavity surfaces, were studied. Some of these protocols produced nearly global chaotic motion, in the sense that the mapping method could detect no regular regions. Other protocols contained large regular islands, and are referred to here as regular flows.

The globally chaotic protocols provided the most rapid mixing, and exhibited a distinct asymptotic behavior at long times. The long-time behavior involved an exponential decrease in both mixing measures, E and σ, with the same time constant. This asymptotic behavior is independent of the sample size used to determine E or σ. Corresponding to this, curves of $E(L)$ and $\sigma(L)$, where L measures the sample size, achieve a self-similar shape in the asymptotic limit. Changing the initial configuration of the two fluids changes the initial rate of mixing, but does not alter the mixing rate or the self-similar behavior in the asymptotic limit.

Regular flows behaved quite differently. They tend to mix much more slowly, and at long times they should approach constant values of E and σ. In fact the mapping results show a slow drift downward from these constant values, because numerical diffusion exchanges some material between the island and its surroundings. For regular flows the degree of mixing at long times is strongly dependent on the initial configuration of the fluids, and particularly on the average content of any islands. For regular protocols there is no self-similarly in $E(L)$ or $\sigma(L)$, and E and σ have different long-time drift rates.

Strictly speaking, the preceding conclusions apply only to the mapping calculation, which is itself an interesting dynamical system. While these results are consistent with our understanding of the mixing behavior of chaotic flows, the calculations shown here do not rigorously demonstrate that fluid flows will exhibit exactly these behaviors. The numerical diffusion present in the mapping method clearly affects the decay rate for E and σ. From the scientific viewpoint the observations made here present an interesting suggestion about the nature of distributive mixing in chaotic flows, a suggestion that might be supported by other types of calculations. The mapping method has provided a facile tool with which one can rapidly explore different mixing protocols, and which can probe the late stages of mixing in which self-similar behavior seems to arise. For the engineering viewpoint, the mapping method is a powerful tool for comparing different mixing flows. It readily distinguishes between flows that are close to globally chaotic and flows with large regular regions, and it also distinguishes between more and less effective chaotic protocols. So long as one compares protocols that use the same number of mapping steps, by using the same displacement per step D, one can expect the relative results to be meaningful.

Regardless of whether the behaviors reported here are physical characteristics of chaotic mixing flows, or are limited to the mapping calculation itself, we have accomplished the main goal of this work. $E(L)$ and $\sigma(L)$ have been shown to provide meaningful measures of distributive mixing, and they can be used to study the nature and progress of mixing processes in a quantitative way.

Acknowledgements

This work was conducted while one of the authors (CLT) was a visiting scholar at the Eindhoven University of Technology, and he gratefully acknowledges financial support from the Dutch Polymer Institute, together with the hospitality of the Materials Technology group (MaTe). The mapping method and the software used here were developed with Alexei Galaktionov, Patrick Anderson, Peter Kruijt, and Han Meijer. We thank them for their assistance, as well as for many interesting suggestions and comments.

References

Aref, H., 1984, Stirring by chaotic advection, *J. Fluid Mech.* **143**, 1-21.

Aref, H. and M.S. El Naschie, eds., 1995, Chaos Applied to Fluid Mixing, Pergamon, reprinted from *Chaos, Solitons and Fractals* **4**(6).

Chella, R. and J. Viñals, 1996, Mixing of a two-phase fluid by cavity flow, *Phys. Rev. E* **53**, 3832-3840.

Chien, W.-L., H. Rising and J.M. Ottino, 1986, Laminar mixing and chaotic mixing in several cavity flows, *J. Fluid Mech.* **170**, 355-377.

Danckwerts, P.V., 1952, The definition and measurement of some characteristics of mixtures, *Appl. Sci. Res.* **A3**, 279-296.

Galaktionov, O.S., P.D. Anderson, G.W.M. Peters and H.E.H. Meijer, 2002a, Mapping approach for 3D laminar mixing simulations: application to industrial flows, *Int. J. Num. Meth. Fluids* **40**, 345-351.

Galaktionov, O.S., P.D. Anderson, G.W.M. Peters and C.L. Tucker, 2002b, A global, multiscale simulation of laminar fluid mixing: the extended mapping method, *Int. J. Multiphase Flow* **28**, 497-523.

Galaktionov, O.S., P.D. Anderson, G.W.M. Peters and F.N. van de Vosse, 2000, An adaptive front tracking technique for three-dimensional transient flows, *Int. J. Num. Meth. Fluids* **32**, 201-219.

Jones, S.W., 1991, The enhancement of mixing by chaotic advection, *Phys. Fluids A* **3**, 1081-1086.

Kruijt, P.G.M., O.S. Galaktionov, P.D. Anderson, G.W.M. Peters and H.E.H. Meijer, 2001, Analyzing fluid mixing in periodic flows by distribution matrices: Mapping method, *AIChE J.* **47**, 1005-1015.

Leong, C.W. and J.M. Ottino, 1989, Experiments on mixing due to chaotic advection in a cavity, *J. Fluid Mech.* **209**, 463-499.

Liu, M., F.J. Muzzio and R.L. Peskin, 1994a, Quantification of mixing in aperiodic chaotic flows, *Chaos, Solitons and Fractals* **4**, 869-893.

Liu, M., R.L. Peshkin, F.J. Muzzio and C.W. Leong, 1994b, Structure of the stretching field in chaotic cavity flows, *AIChE J.* **40**, 1273-1286.

Meleshko, V.V., 1996, Steady Stokes flow in a rectangular cavity, *Proc. R. Soc. Lond.* **A452**, 1999-2022.

Meleshko, V.V. and G.W.M. Peters, 1996, Periodic points for two-dimensional Stokes flow in a rectangular cavity, *Phys. Lett. A* **216**, 87-96.

Mohr, W.D., R.L. Saxton and C.H. Jepson, 1957, Mixing in laminar-flow systems, *Ind. Eng. Chem.* **49**, 1855-1856.

Muzzio, F.J., P.D. Swanson and J.M. Ottino, 1991, The statistics of stretching and stirring in chaotic flows, *Phys. Fluids A* **3**, 822-834.

Ottino, J.M., 1989, The kinematics of mixing: stretching, chaos and transport, Cambridge University Press.

Scott, A.M. and J. Bridgwater, 1974, The characterization of patchy mixtures, *Chem. Eng. Sci.* **29**, 1789-1800.

Tucker, C.L., 1981, Sample variance measurement of mixing, *Chem. Eng. Sci.* **36**, 1829-1839.

Wetzel, E.D. and C.L. Tucker, 1999, Area tensors for modeling microstructure during laminar liquid-liquid mixing, *Int. J. Multiphase Flow* **25**, 35-61.